Supplementary Information

Deconstructing the black box of zeolite crystallization gels by species-specific isolation

Kexin Yan[†,1], Feng Lin[†,1], Zhaoqi Ye[1], Yifan Zhang[1], Yang Zhao[1], Zhangping Shi[3], Di Pan[1], Yahong Zhang[1], Hongbin Zhang[,2], Yi Tang*[,1]*

[1]*Department of Chemistry, College of Smart Materials and Future Energy, State Key Laboratory of Porous Materials for Separation and Conversion, Shanghai Key Laboratory of Molecular Catalysis and Innovative Materials, and Laboratory of Advanced Materials, Fudan University, Shanghai 200433, P. R. China.*

[2]*Key Laboratory of Silicate Cultural Heritage Conservation (Ministry of Education), Institute for the Conservation of Cultural Heritage, School of Cultural Heritage and Information Management, Shanghai University, Shanghai, 200444, China.*

[3]*State Key Laboratory of Green Chemical Engineering and Industrial Catalysis, SINOPEC Shanghai Research Institute of Petrochemical Technology, Shanghai 201208, China.*

*Correspondence to: yitang@fudan.edu.cn; zhang-hongbin@shu.edu.cn

Content:

1. Materials Synthesis and Characterization

Chemicals:

Silica sol (Ludox, 40 wt%), $NaAlO_2$ (Aladdin, 41% Al_2O_3, 59% Na_2O) and TEAOH (Aladdin, 25 wt% in water) were used to synthesize MTW-*t*-Gel. NH_4NO_3 (Aladdin, Analytical Reagent) were used to synthesize NH_4^+ type samples. Pyridine (99.5%) was purchased from Aladdin Shanghai, China. All the reagents and solvents were used without further purification.

Experimental Section:

Synthesis of samples:

The MTW zeolite is prepared in the gel with the composition of $n_{SiO2}/n_{Al2O3}/n_{Na2O}/n_{TEAOH}/n_{H2O}$ = 100/ 0.83/ 1.73/ 16/ 1000. In detail, TEAOH solution is firstly mixed with deionized water under mechanical stirring. Then, sodium aluminate is added into the mixture and stirred until the solution is clear. Followed by the dropwise adding of silica sol, the mixture condenses to gel at the beginning and then turns transparent quickly with the addition of the silica sol in mixture. After 3 hours aging at room temperature, the resulting solution (pH = 12.5) is transferred into a Teflon-lined autoclave and heated at 160 °C for *t* hours. After hydrothermal treatment, the products are cooled in water bath and called MTW-*t*. The MTW-72 sample is a product that undergoes a complete crystallization process after 72 hours of hydrothermal treatment in the system, followed by centrifugation and drying.

The "deconstruction-dialysis" method to deconstruct the gel:

To obtain varied aluminosilicate samples with different physicochemical properties and investigate the crystallization mechanism, the gel has to be deconstructed due to the complex compositions which are tightly aggregated. The specific deconstruction and separation process needs to go through two steps. Firstly, the directly synthesized MTW-*t* sample is vacuum dried at -50 °C to gain the MTW-*t*-Gel sample. The MTW-*t*-Gel sample is dispersed in a certain amount of water to remove soluble species, then centrifuged to obtain the solid species and vacuum dried at -50 °C.

Next, for the sake of deconstructing the gel, the MTW-*t*-Gel sample then mixes with 0.8 M TEAOH solution in the solid liquid mass ratio of 1:15 for 6 hours at room temperature. Here, the ample TEAOH solution is used to ensure the gel completely broken down. Meanwhile, owing to the protection of TEA^+ groups and mild conditions

(low temperature and the mixed solution's pH = 11.5, lower than the initial synthesis solution), the ordered precursors can retain their microstructure as much as possible. The resulting mixture is then centrifuged at 10000 rpm for 6 minutes, yielding large particles named MTW-*t*-C and dried at 80 °C.
Subsequently, a two-step dialysis is employed to further separate aluminosilicate precursors with different thermodynamic properties in the upper suspension. Specifically, the supernatant after centrifugation is put into the dialysis film and seal it with clips. Then, the dialysis bag is slowly stirred in the first dialysis liquor (9 mM TEAOH solution) for 24 hours, followed by the second dialysis liquor (deionized water) until the pH of the external liquor is close to neutral. The species in dialysis bags are freeze-dried, gaining MTW-*t*-HOP (Highly ordered precursor) sample.

Characterization and Computation:
X-ray diffraction (XRD): The X-ray diffraction (XRD) patterns from 5 to 50° are obtained from a Bruker D2-Advanced diffractometer (Cu-Kα, 10 kV, 30 mA).

The infrared spectrum (IR): The infrared spectrum (IR) experiments are performed on a PerkinElmer Frontier infrared spectrometer.

Scanning electron microscope (SEM): The SEM images are collected from the field-emission scanning electron microscopy (Zeiss Gemini SEM500 FESEM).

Transmission electron microscope (TEM): The TEM images are conducted on the field-emission transmission electron microscope (FE-TEM, Tecnai G2 F20 S-Twin) to observe the structure features.

Dynamic light scattering (DLS): The Nano-ZS90 zetasizer is used to monitor the changes of samples' particle size by dynamic light scattering (DLS). To ensure the validity of the data, the dispersion of the sample needs an extremely dilute concentration.

Physical adsorption instrument: The Ar-sorption experiments of calcined samples are measured on a Quantachrome iQ-2 instrument at 87 K after outgassing at 573 K for 8 hours which can detailedly characterize the porous structure in micro and mesoscopic.

Inductively coupled plasma-atomic emission spectrometry (ICP-AES): The differences of the elements in the whole sample are tested by inductively coupled plasma-atomic emission spectrometry (ICP-AES, iCAP 7400).

X-ray Photoelectron Spectroscopy (XPS): The surface elemental composition of samples is measured by X-ray Photoelectron Spectroscopy (XPS, Scientific Escalab 250Xi Spectrometer).

Ultraviolet Raman spectroscopy (UV-Raman): The Horiba Jobin Yvon XploRA confocal microscope with a laser source of 244 nm is applied to collect the UV-Raman data.

Magic angle spinning nuclear magnetic resonance (MAS NMR): The status of silicon or aluminum in zeolite is characterized by solid-state MAS NMR (Bruker DSX 300).

Thermogravimetric-mass spectroscopic (TG): Thermogravimetric spectroscopic (TG) was performed on an SDT Q650-GSD 301 T2 hyphenated instrument with air (100 ml/min).

NH_3-temperature programmed desorption (NH_3-TPD): The acid content of the sample was evaluated by NH_3-TPD test on the AutoChem II 2920 instrument (Micromeritics Company).

Pyridine adsorption infrared test (Py-IR): The testing instruments used in the pyridine adsorption infrared (Py-IR) test were Nicolet 6700 (Thermo Fisher) and INVENIOS (Bruker).

The growth and crystallization process of the system:
The growth and crystallization process of the system is described using the following parameters: (1) the crystallization curve of the whole system, (2) the relative yield or volume of MTW-*t*-C, and (3) the absolute yield of MTW-*t*-C, MTW-*t*-HOP, MTW-*t*-POP and the soluble monomers and oligomers. The specific calculation methods are as follows: the relative crystallinity of the MTW-*t*-Gel sample is calculated by the relative peak area between 2θ = 6.7 ~ 9.4 ° and 18.5 ~ 24.0 ° compared with the final MTW-72 sample. The yield of MTW-*t*-C sample is the weight of MTW-*t*-C solid sample (after calcination to remove the SDA and water) divided by weight of original MTW-*t*-Gel sample. Similarly, the yield of MTW-*t*-HOP sample is calculated from the weight of solid calcinated MTW-*t*-HOP sample and original MTW-*t*-Gel sample. Moreover, the relative yield of the MTW-*t*-C sample is the yield of the MTW-*t*-C sample divided by the yield of the MTW-72. The mass loss of solid species in the first washing process is defined as the yield of monomers/oligomers. The yield of MTW-*t*-POP samples is the total amount (value of 100%) minus the yield of MTW-*t*-C, MTW-*t*-HOP samples, monomers/oligomers and the water and SDA content tested by TG.

Explanation of the Avrami equation[1-4]:

In the Avrami equation $\alpha=1-e^{-k(t-t_0)^n}$, α is the proportion of transformed phase ($0 \leq \alpha \leq 1$), k is the reaction rate constant, t is the crystallization time, t_0 is the induction period, n is the crystallization index, whose value is directly related to the crystallization

mechanism. And n can be expressed as the function of the number of crystal growth dimensions (ξ) and the correlation between nucleation time (δ), namely n = ξ + δ. The ξ value is decided by growth patterns. When δ = 0, it means an instantaneous nucleation.

Nucleation behavior calculation:

Considering that after 40 hours, the particle diameter of MTW-*t*-C no longer increases, but the yield still increases, so the volume at 40 hours is selected as the benchmark to analyze the nucleation at the particle attachment stage.

To facilitate the comparison of changes, the ratio of the relative yield (RY) to the relative volume (RV) at 40 h is defined as 1 artificially. From this, the RV at other time points relative to 40 h can be calculated by their diameters:

$$RV_t = \left(\frac{\bar{d}_t}{\bar{d}_{40}}\right)^3 \cdot RV_{40}.$$

Next, consider the changes in the crystal nuclei at any different times in 24-40 h. The physical quantities involved in the formula are shown in the following table.

From 40-△t moment to 40 h, the size of the original nucleus changes by △d. And the size changes at a constant rate, so suppose that there are △n nuclei increasing in △t hours, and their size is △d.

Considering that the average volume-average value measured by DLS was used to calculate the volume in the experiment, the volume-weighted average particle size was also used to calculate the volume in the derivation process.

Moment	Size	Number of nuclei	Average size
40-△t	d	n	$\bar{d}_{40\text{-}\Delta t}=d$
40	d+△d	n	$\bar{d}_{40}=\frac{n(d+\Delta d)^4+\Delta n\Delta d^4}{n(d+\Delta d)^3+\Delta n\Delta d^3}$
	△d	△n	

Then the relative yield at moment 40-△t and 40 h =

$$\frac{RY_{40\text{-}\Delta t}}{RY_{40}}=\frac{nd^3\rho}{n(d+\Delta d)^3\rho+\Delta n(\Delta d)^3\rho}$$

The relative volume at moment 40-△t and 40 h =

$$\frac{RV_{40\text{-}\Delta t}}{RV_{40}}=\left(\frac{\bar{d}_{40\text{-}\Delta t}}{\bar{d}_{40}}\right)^3=\frac{d^3(n(d+\Delta d)^3+\Delta n\Delta d^3)^3}{\left(n(d+\Delta d)^4+\Delta n\Delta d^4\right)^3}$$

Because $\frac{RY_{40}}{RV_{40}}=1$ is set by us in advance artificially,

$$\frac{RY_{40-\Delta t}}{RV_{40-\Delta t}}=\frac{RY_{40-\Delta t}}{RY_{40}}\div\frac{RV_{40-\Delta t}}{RV_{40}}=\frac{n(n(d+\Delta d)^4+\Delta n\Delta d^4)^3}{\left(n(d+\Delta d)^3+\Delta n\Delta d^3\right)^4}$$

$$=\frac{(d+\Delta d)^{12}n^4+3(d+\Delta d)^8\Delta d^4\Delta n\cdot n^3+3(d+\Delta d)^4\Delta d^8\Delta n^2\cdot n^2+\Delta d^{12}\Delta n^3\cdot n}{(d+\Delta d)^{12}n^4+4(d+\Delta d)^9\Delta d^3\Delta n\cdot n^3+6(d+\Delta d)^6\Delta d^6\Delta n^2\cdot n^2+4(d+\Delta d)^3\Delta d^9\Delta n^3\cdot n+\Delta d^{12}\Delta n^4}\quad\text{（S1）}$$

For this polynomial with respect to n, it is constant only if △n=0

$$\frac{RY}{RV}=\frac{(d+\Delta d)^{12}n^4}{(d+\Delta d)^{12}n^4}=1$$

2. Supplementary Figures and Tables.

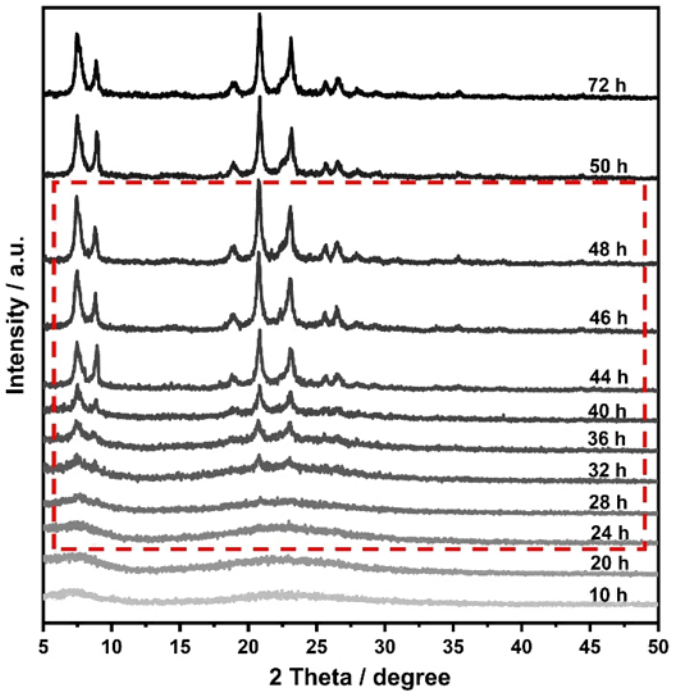

Fig. S1 The XRD patterns of MTW-*t*-Gel samples with different hydrothermal times.

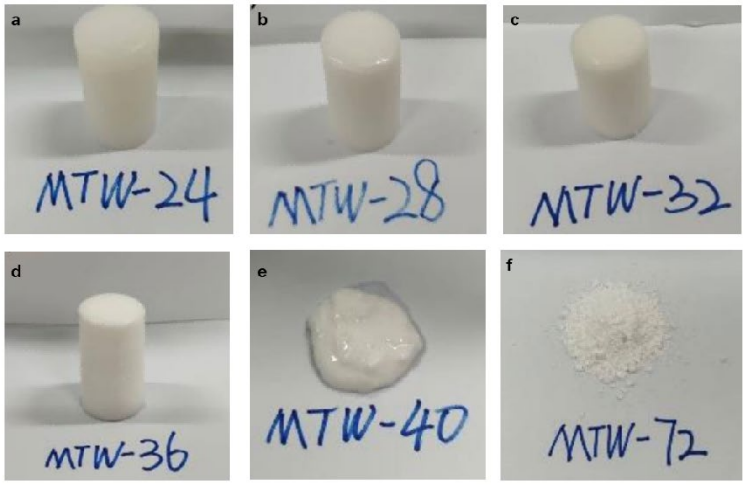

Fig. S2 The optical photo of MTW-*t*-Gel before freeze-drying, where *t* = (a)24 / (b) 28 / (c) 32 / (d) 36 / (e) 40 and (f) freeze-dried MTW-72.

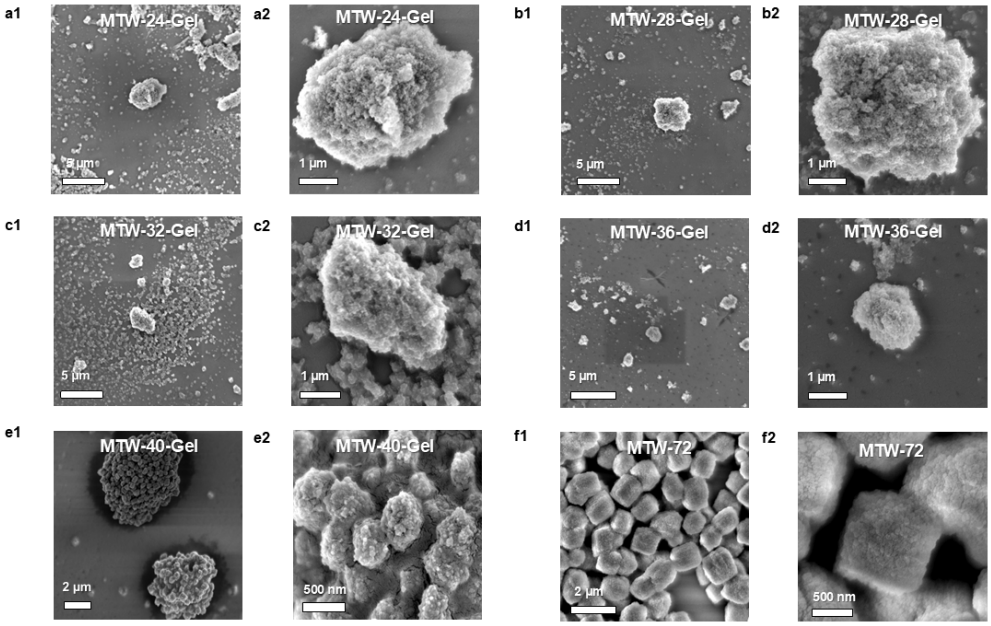

Fig. S3 The SEM image of MTW-*t*-Gel, where *t* = (a) 24 / (b) 28 / (c) 32 / (d) 36 / (e) 40 and (f) freeze-dried MTW-72.

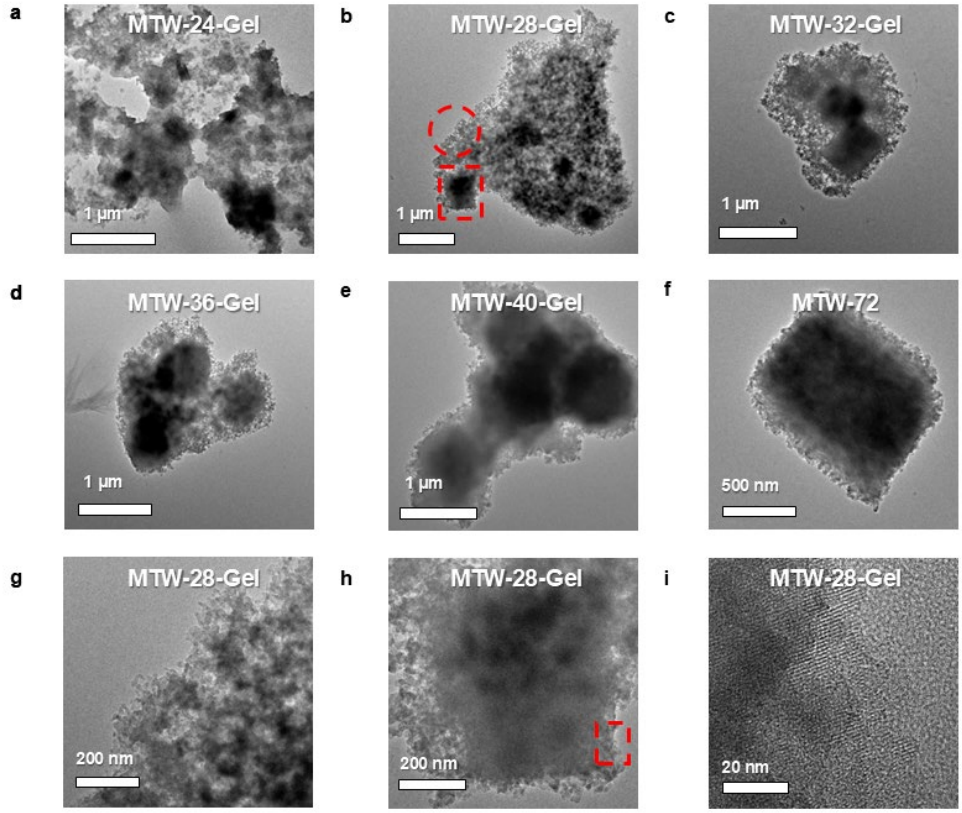

Fig. S4 The TEM image of MTW-*t*-Gel, where *t* = (a)24 / (b) 28 / (c) 32 / (d) 36 / (e) 40 and (f) freeze-dried MTW-72. The detail image of MTW-28-Gel is shown in figure g / h / i.

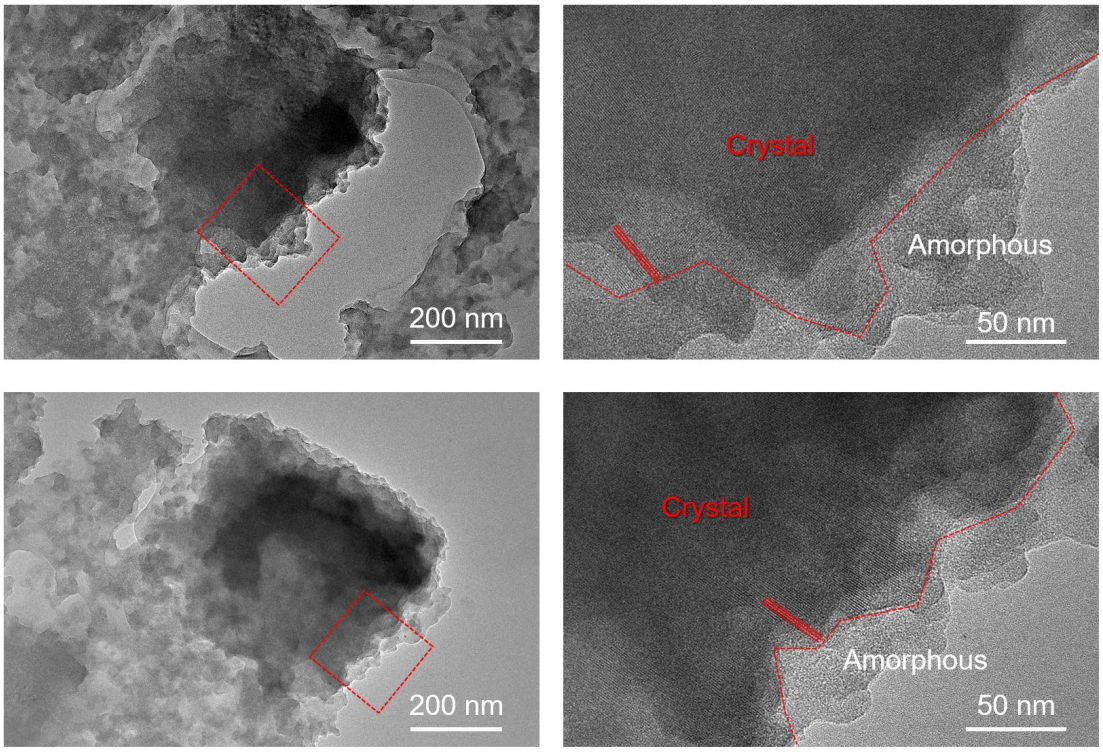

Fig. S5 The TEM images of sliced MTW-28-Gel.

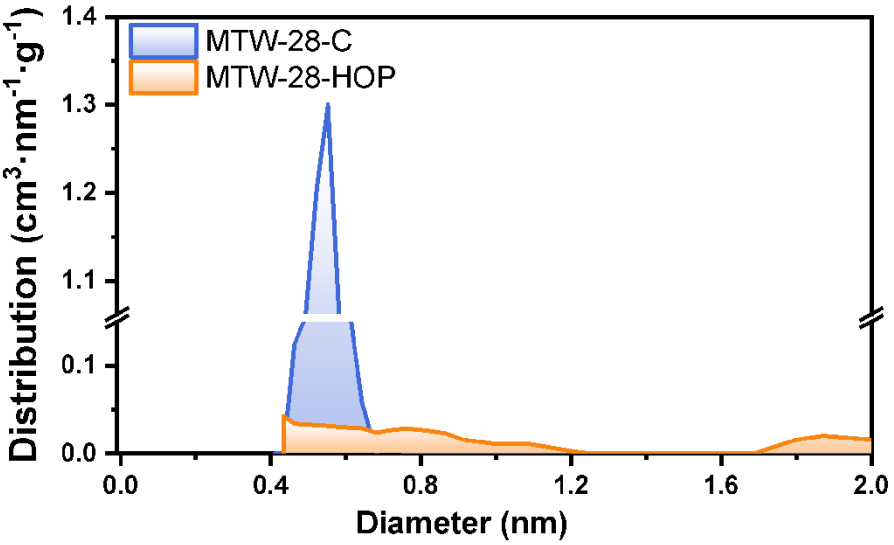

Fig. S6 The pore size distribution of the micropore segments of MTW-28-C and MTW-28-HOP

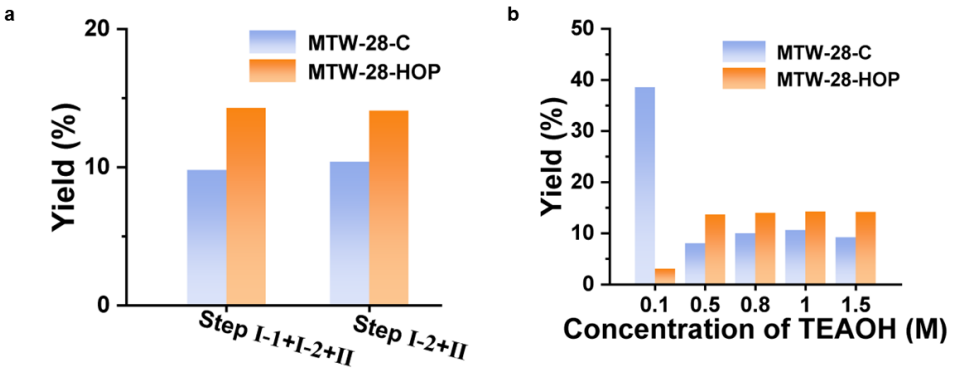

Fig. S7 The species yield after (a) changing the operation steps or the (b) concentration of TEAOH.

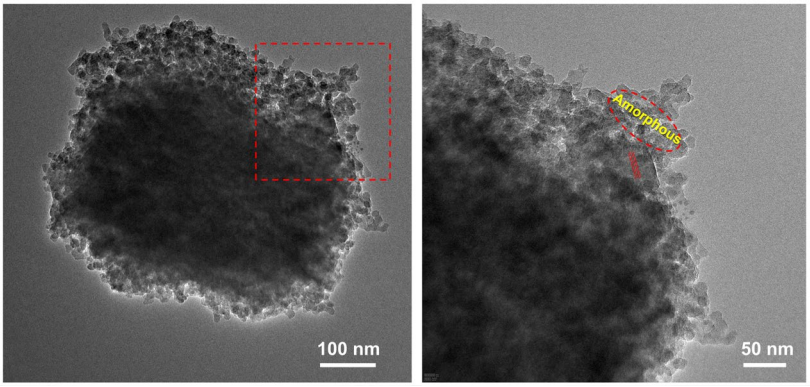

Fig. S8 TEM images of the sample obtained by centrifugation under the deconstruction condition of 0.1 M TEAOH

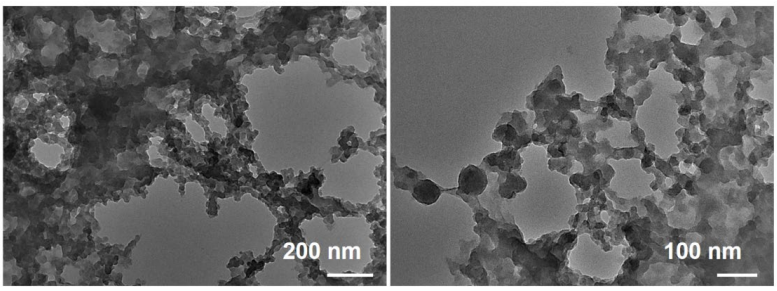

Fig. S9 TEM images of the samples before dialysis.

Table S1. The texture properties of MTW-*t*-C zeolite

	S_{BET}[a] (m^2/g)	S_{micro}[b] (m^2/g)	S_{ext}[b] (m^2/g)	V_{micro}[c] (cm^3/g)	V_{meso}[c] (cm^3/g)	V_{total}[c] (cm^3/g)
t = 24	352	116	236	0.118	0.475	0.593
t = 28	333	145	189	0.130	0.236	0.366
t = 32	333	160	173	0.133	0.227	0.361
t = 36	298	136	163	0.115	0.215	0.330
t = 40	310	115	195	0.114	0.259	0.373
t = 44	352	210	142	0.153	0.214	0.367
t = 48	352	231	121	0.160	0.210	0.370
t = 72	359	225	134	0.164	0.140	0.304

[a] determined by the multi-point BET; [b] t-plot method;
[c] by DFT model, model: Ar at 87 K zeolites/silica (cylinder. pores, NLDFT ads.).

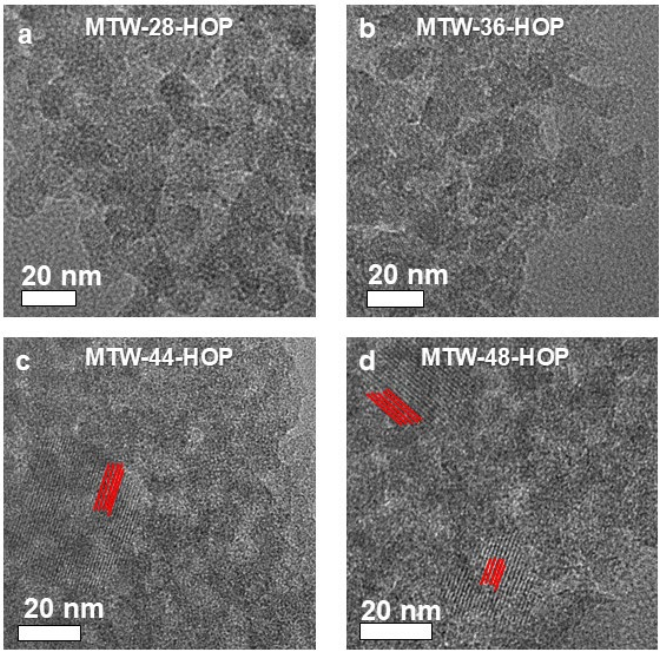

Fig. S10 The TEM images of MTW-*t*-HOP samples, where *t* = (a) 28 / (b) 36 / (c) 44 / (d) 48.

Table S2. The texture properties of MTW-*t*-HOP aluminosilicate precursors

	S_{BET}[a] (m^2/g)	S_{micro}[b] (m^2/g)	S_{ext}[b] (m^2/g)	V_{micro}[b] (cm^3/g)	V_{meso}[b] (cm^3/g)	V_{total}[b] (cm^3/g)
t = 24	323	140	294	0.0289	0.967	0.970
t = 28	375	120	347	0.0222	0.941	0.943
t = 32	376	164	335	0.0256	0.856	0.859
t = 36	374	194	335	0.0266	0.788	0.791
t = 40	440	100	390	0.0119	0.680	0.681

[a] determined by the multi-point BET;

[b] by DFT model, model: Ar at 87 K zeolites/silica (cylinder. pores, NLDFT ads.);

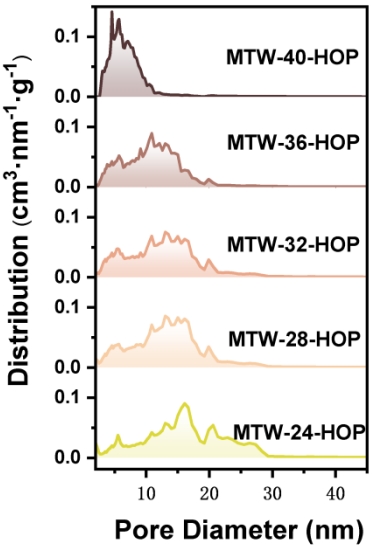

Fig. S11 The pore size distribution of MTW-*t*-HOP samples in the mesopore (2~50 nm) sections by DFT model.

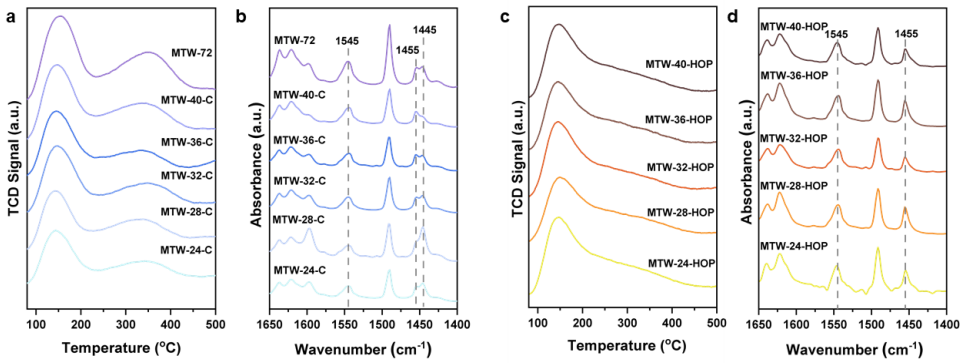

Fig. S12 The (a) NH_3-TPD and (b) Py-IR spectrum of MTW-*t*-C. And The (c) NH_3-TPD and (d) Py-IR spectrum of MTW-*t*-HOP.

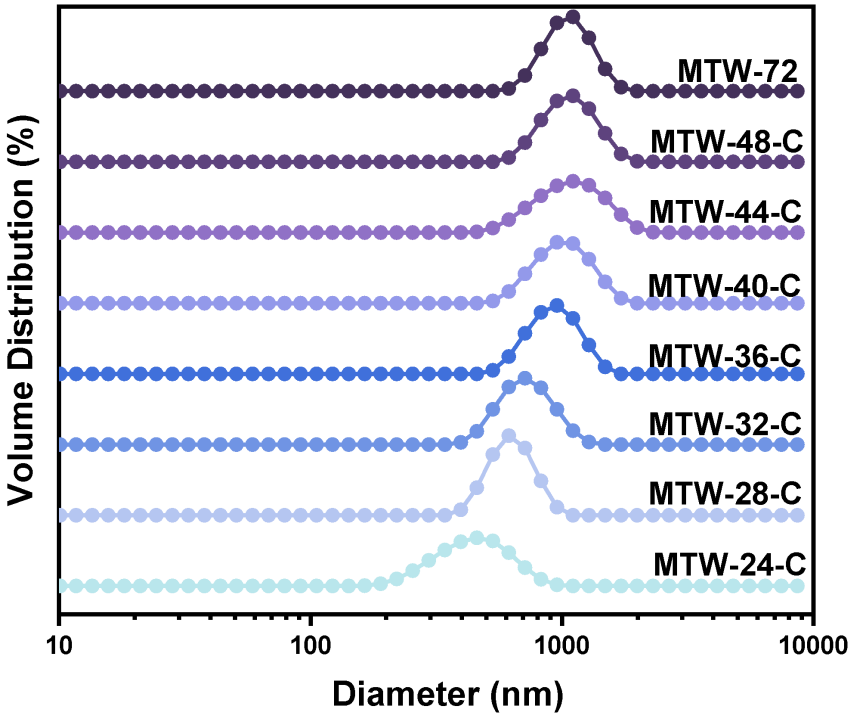

Fig. S13 The DLS particle size distribution of MTW-*t*-C samples with different hydrothermal times.

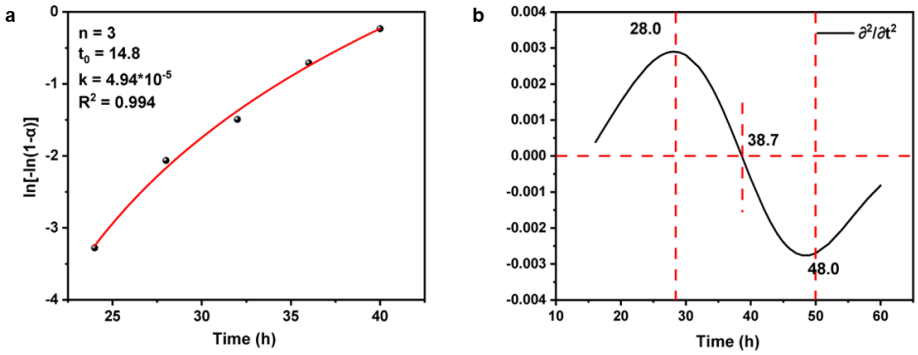

Fig. S14 (a) The logarithmically fitted Avrami equation when α is the relative yield of MTW-*t*-C during 24~40 hours of hydrothermal treatment; (b) The second derivative of the fitted curve.

Table S3. The Si/Al ratios of different regions in the MTW-40-C and MTW-72 sample's cross-section

	Time (h)	Spectrum					
		1	2	3	4	5	6
Si/Al Ratio	40	61	170	275	186	56	38
	72	60	123	226	244	152	46

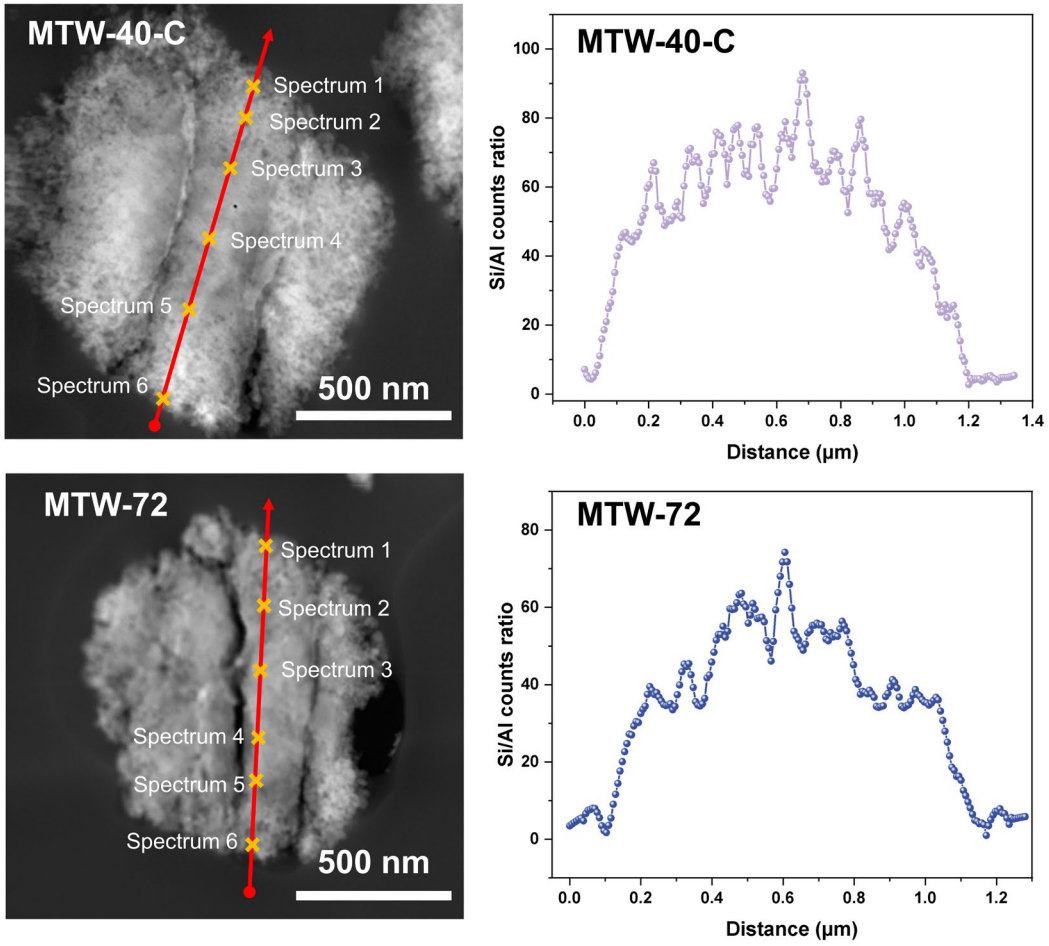

Fig. S15 The TEM image of the MTW-40-C and MTW-72 sample's cross-section, and the elemental line-scan profiles of different regions.

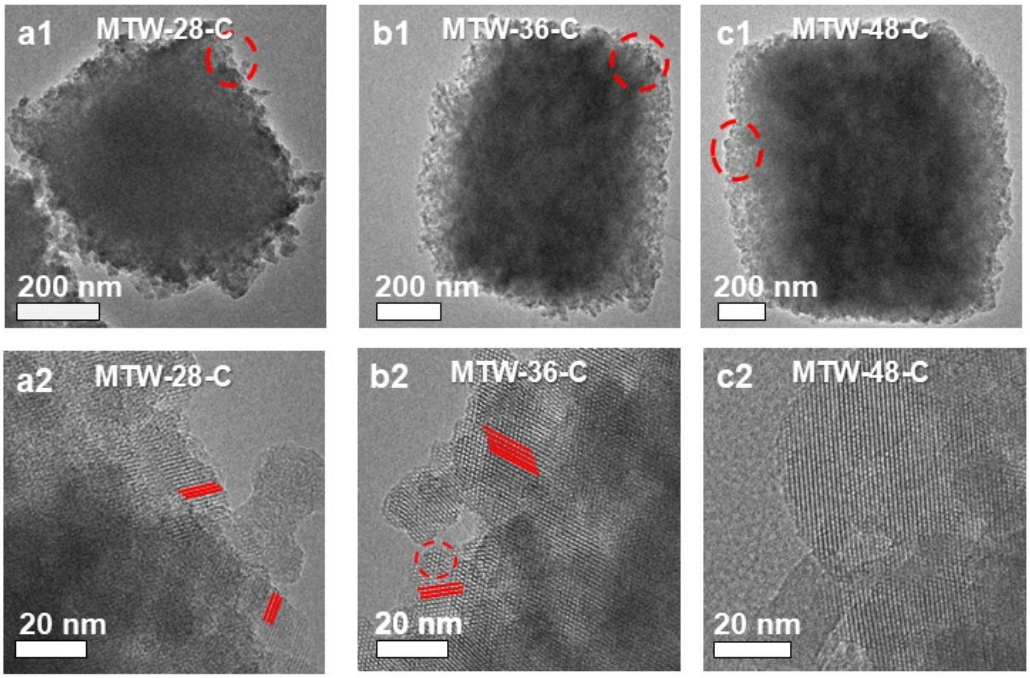

Fig. S16 The TEM images of MTW-*t*-C zeolite crystals, where t = (a) 28 / (b) 36 and (c) 48, and the detailed images of the region in the red circles of the figure 1 series are shown in Figure 2 series.

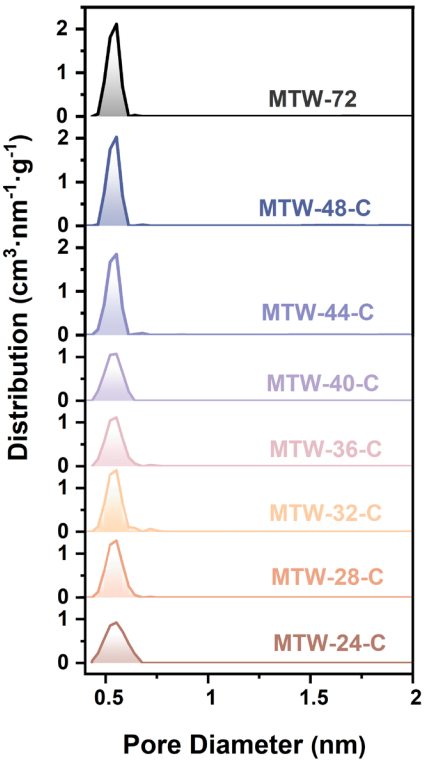

Fig. S17 The pore size distribution of MTW-*t*-C samples in the micropore (0~2 nm) sections by DFT model.

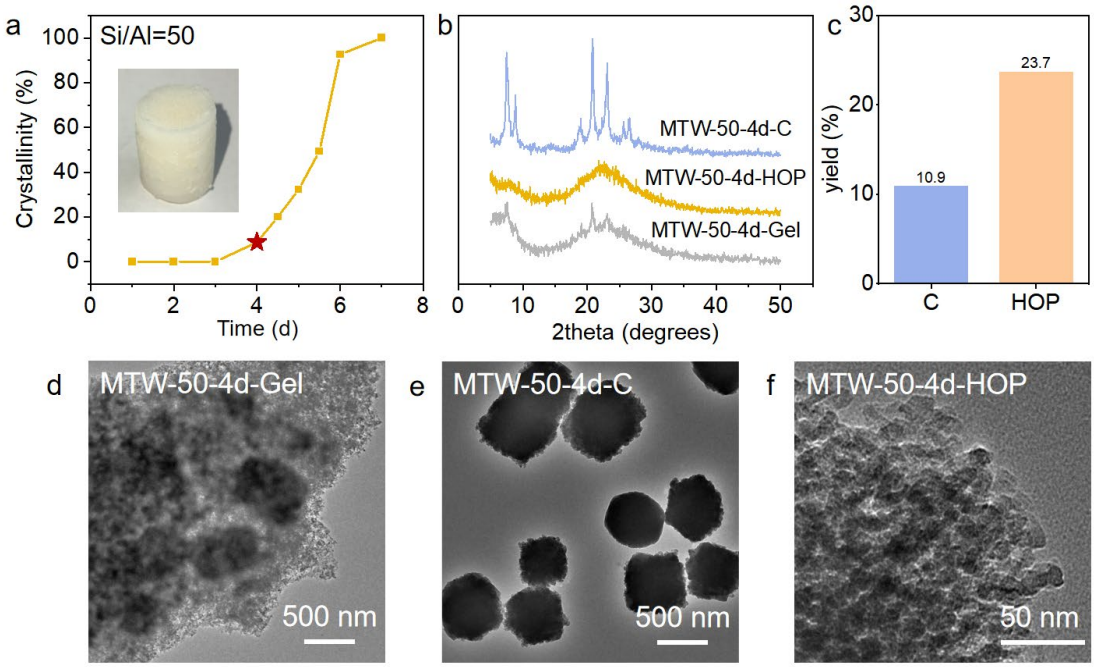

Fig. S18 (a) The crystallization kinetics curve with the input Si/Al ratio of 50, calculated from the XRD relative crystallinity. Inset is an optical photograph of the gel. The (b) XRD pattern and (c) the yield of the MTW-50-4d-Gel, MTW-50-4d-C and MTW-50-4d-HOP species. TEM images of (d) MTW-50-4d-Gel, (e) MTW-50-4d-C and (f) MTW-50-4d-HOP species obtained by "deconstruction-dialysis" method.

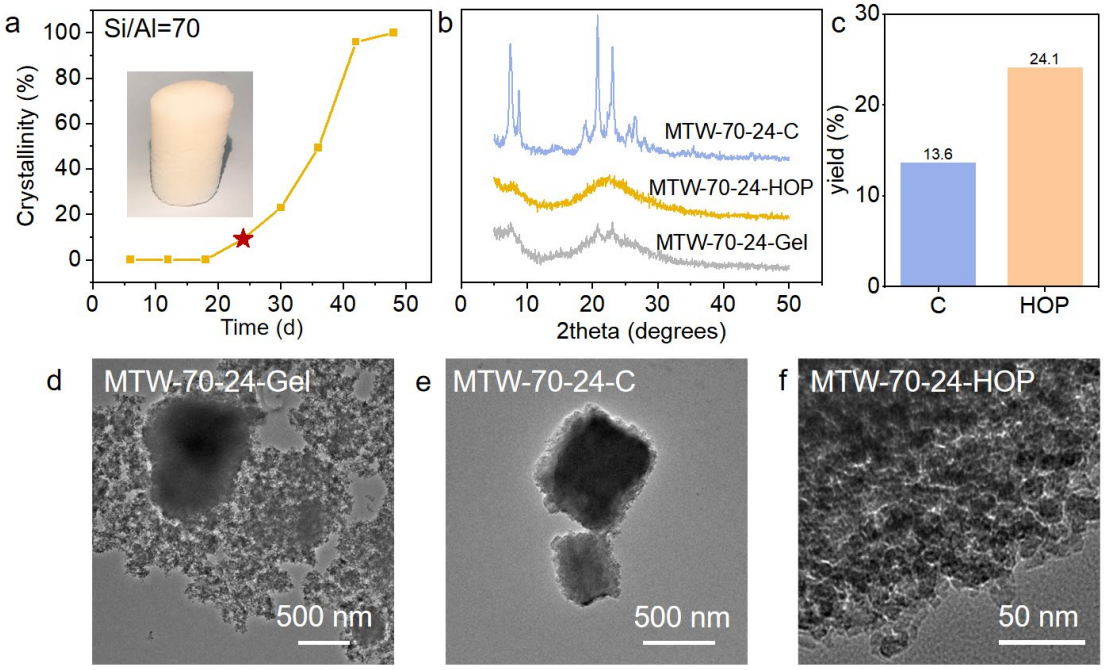

Fig. S19 (a) The crystallization kinetics curve with the input Si/Al ratio of 70, calculated from the XRD relative crystallinity. Inset is an optical photograph of the gel. The (b) XRD pattern and (c) the yield of the MTW-70-24-Gel, MTW-70-24-C and MTW-70-24-HOP species. TEM images of (d) MTW-70-24-Gel, (e) MTW-70-24-C and (f) MTW-70-24-HOP species obtained by "deconstruction-dialysis" method.

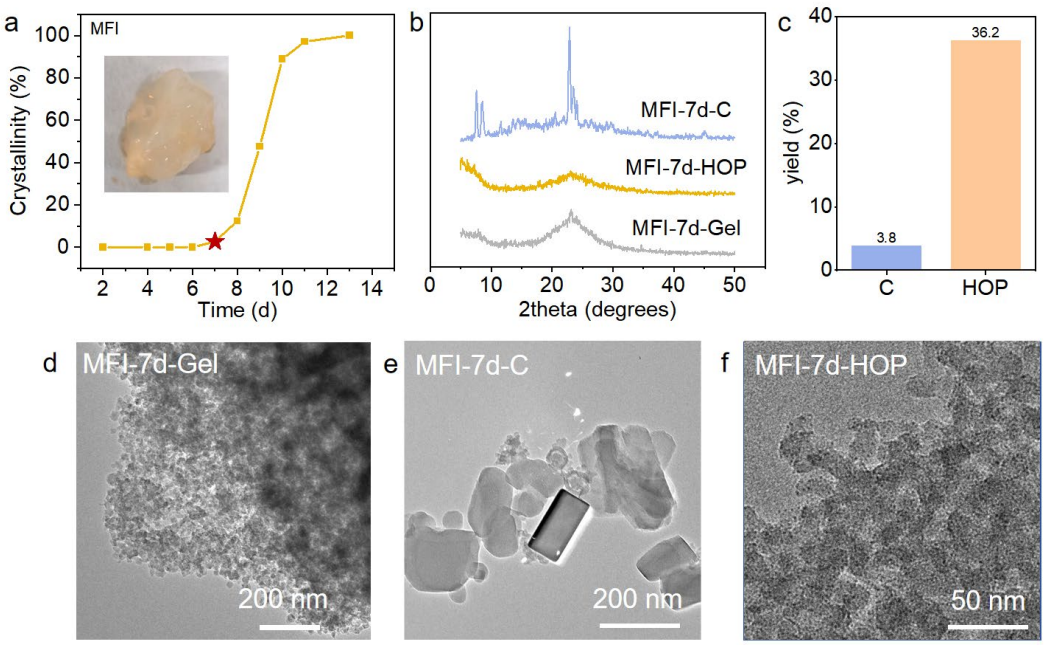

Fig. S20 (a) The crystallization kinetics curve calculated from the XRD relative crystallinity. Inset is an optical photograph of the gel. The (b) XRD pattern and (c) the yield of the MFI-7d-Gel, MFI-7d-C and MFI-7d-HOP species. TEM images of (d) MFI-7d-Gel, (e) MFI-7d-C and (f) MFI-7d-HOP species obtained by "deconstruction-dialysis" method.

3. References.

1 M. Tomellini and M. Fanfoni, Connection between phantom and spatial correlation in the Kolmogorov–Johnson–Mehl–Avrami-model: A brief review, *Physica A,* 2022, **590**, 126748.

2 P. F. Corregidor, D. E. Acosta and H. A. Destéfanis, Kinetic Study of Seed-Assisted Crystallization of ZSM-5 Zeolite in an OSDA-Free System Using a Natural Aluminosilicate as Starting Source, *Ind. Eng. Chem. Res.,* 2018, **57**, 13713.

3 R. W. Thompson, Analysis of zeolite crystallizations using Avrami transformation methods, *Zeolites,* 1992, **12**, 680.

4 P. Zhang, S. Li, P. Guo and X. Zhao, Synthesis of ZSM-5 Microspheres Made of Nanocrystals from Iron Ore Tailings by the Solid-Phase Conversion Method, *Langmuir,* 2020, **36**, 6160.